A DESI DR1 Radial-Velocity Search for Dark Compact Companions: A Strong but Unconfirmed Candidate Around a dM0 Star

Aiden Smith (A.I Sloperator)

January 16, 2026

Abstract

We present a conservative, fully reproducible search for radial-velocity (RV) variability in the public Dark Energy Spectroscopic Instrument (DESI) Data Release 1 (DR1) Milky Way Survey. Using only per-epoch RV measurements, we identify stars whose velocity variability is both highly significant and robust under leave-one-out tests. A "negative space" validation pipeline then rejects ordinary luminous companions using Gaia DR3 astrometry, WISE infrared photometry, GALEX ultraviolet imaging, TESS and ZTF time-domain photometry, deep Legacy Survey imaging, and archival X-ray and radio catalogs.

One system, Gaia DR3 3802130935635096832, emerges as a strong dark companion candidate. Combining one LAMOST epoch with four DESI epochs yields a $146.07\,\mathrm{km\,s^{-1}}$ RV span over a 5.9 yr baseline. A conservative significance metric gives $S_{\rm robust} \simeq 33$ and the constant-RV hypothesis is rejected at $\Delta\chi^2 \simeq 2.7 \times 10^4$. Injection–recovery tests show that such a large improvement over a constant model never arises in 1000 noise-only realizations with identical sampling. Gaia DR3 reports RUWE $\simeq 1.95$ and significant astrometric excess noise, consistent with unresolved orbital motion but also compatible with a marginal blend.

Using LAMOST spectral typing we infer a primary mass $M_1 = 0.56 \pm 0.06\,\mathrm{M}_\odot$ and derive a RV mass function $f(M) \simeq 1.95\,\mathrm{M}_\odot$ from MCMC fits to the five epochs. The resulting minimum companion mass distribution has median $M_{2,\rm min} \simeq 2.8\,\mathrm{M}_\odot$ with a 16–84 % range 1.2–4.3 $\mathrm{M}_\odot$; we find an $\approx 82\%$ probability that the companion is heavier than $1.4\,\mathrm{M}_\odot$ and a $\approx 45\%$ probability that it exceeds $3\,\mathrm{M}_\odot$. X-ray and radio non-detections imply a luminosity well below typical quiescent neutron stars or stellar-mass black holes, and ZTF photometry rules out starspot-induced RV variability at the required level. However, period recovery from five RV epochs is intrinsically aliased, and injection–recovery simulations show that only $\sim 17\%$ of true 15–30 day signals are recovered at the correct period with this sampling.

We therefore classify Gaia DR3 3802130935635096832 as a *strong but unconfirmed* dark compact companion candidate. The evidence strongly favors a non-luminous object more massive than any ordinary star that the data would have revealed, but the orbit and dynamical mass remain underdetermined. A small number of additional high-resolution RV measurements would be sufficient to confirm or refute the compact-object interpretation.

1 Introduction

Quiescent compact objects—white dwarfs (WDs), neutron stars (NSs), and stellar-mass black holes (BHs)—are expected to be abundant in the Milky Way but are difficult to detect when not accreting or otherwise luminous. Radial velocities provide a purely gravitational discovery channel: a compact companion can induce large reflex motion in an ordinary star while contributing negligible

light. Modern multi-epoch spectroscopic surveys are therefore natural hunting grounds for unseen companions.

DESI DR1 provides per-epoch RVs for millions of stars in the Milky Way Survey. While DESI was not designed as a time-domain survey, the combination of multi-epoch coverage, high spectral resolution, and uniform data processing enables a systematic search for RV outliers. In this work we:

1. define conservative RV-variability metrics that are robust to outliers;
2. scan the DESI DR1 Milky Way Survey for high-significance RV variables;
3. apply a multi-wavelength "negative space" filter that searches for *gravity without light*;
4. perform targeted orbital and population-level analyses of the strongest surviving candidate, including extensive stress testing against alternative explanations.

All analysis scripts, configuration files, and machine-readable products are publicly available at `https://github.com/simulationstation/DESI-BH-CANDIDATE-SEARCH`. The goal is not to claim a definitive compact-object discovery from public data alone, but to identify and characterize the most promising targets for follow-up.

2 Data Sets

2.1 DESI DR1 Milky Way Survey

We use per-epoch DESI DR1 Milky Way Survey RVs from the `main-bright` and `main-dark` programs. For each epoch we extract:

- heliocentric radial velocity RV_i (in $\mathrm{km\,s^{-1}}$);
- formal RV uncertainty $\sigma_{\mathrm{RV},i}$ (in $\mathrm{km\,s^{-1}}$);
- modified Julian date t_i (in days);
- DESI `TARGETID`;
- Gaia DR3 `SOURCE_ID` when available.

2.2 LAMOST Archival Spectroscopy

A query of public LAMOST DR7 reveals one additional medium-resolution spectrum of Gaia DR3 380213093563509 taken on MJD 57457 with $\mathrm{RV} = -49.36 \pm 2.79$ $\mathrm{km\,s^{-1}}$ and spectral classification dM0. We adopt this as an independent pre-DESI RV epoch and as the primary spectral-type constraint.

2.3 Gaia DR3 Astrometry

From Gaia DR3 we use:

- parallax $\varpi = 0.12 \pm 0.16$ mas;
- proper motions;

- renormalized unit weight error (RUWE) $\simeq 1.95$;
- astrometric excess noise (AEN) $\epsilon_{\rm AEN} \simeq 0.90$ mas;
- image-parameter-determination (IPD) summary statistics, including `ipd_frac_multi_peak` $\simeq 8\%$.

The parallax is too uncertain for a precise geometric distance, so we instead adopt a spectro-photometric distance of $d \simeq 495 \pm 91$ pc derived from the LAMOST-based stellar parameters.

2.4 Additional Surveys

The multi-wavelength validation makes use of:

- WISE/2MASS photometry for infrared colours;
- GALEX NUV imaging for hot WD signatures;
- TESS full-frame-image photometry;
- ZTF multi-year g, r photometry;
- Legacy Survey (DECaLS/MzLS/BASS) imaging cutouts;
- ROSAT, XMM-Newton, Chandra X-ray catalogs;
- NVSS, FIRST, and VLASS radio surveys.

All cross-matching and archive queries are scripted and version-controlled.

3 RV Variability Metrics

3.1 Single-target RV statistics

For each target with N RV epochs we define the maximum observed RV span

$$\Delta \mathrm{RV}_{\max} = \max_i \left(\mathrm{RV}_i\right) - \min_i \left(\mathrm{RV}_i\right). \tag{1}$$

Table 1: Definitions for Equation (1).

Symbol	Meaning
RV_i	Radial velocity at epoch i (in $\mathrm{km\,s^{-1}}$)
$\Delta \mathrm{RV}_{\max}$	Maximum difference between any two epoch RVs (in $\mathrm{km\,s^{-1}}$)
$\max_i(\cdot)$, $\min_i(\cdot)$	Maximum and minimum over all epochs i

To quantify the significance of the variability we define

$$S = \frac{\Delta \mathrm{RV}_{\max}}{\sqrt{\sum_{i=1}^{N} \sigma_{\mathrm{RV},i}^2}}. \tag{2}$$

Table 2: Definitions for Equation (2).

Symbol	Meaning
S	Global RV-variability significance (dimensionless)
$\Delta\mathrm{RV}_{\max}$	As in Equation (1)
$\sigma_{\mathrm{RV},i}$	Formal RV uncertainty at epoch i (in $\mathrm{km\,s^{-1}}$)
N	Number of RV epochs used in the sum

3.2 Leave-one-out robustness and leverage

Because a single bad epoch can inflate S, we compute a leave-one-out significance $S^{(-k)}$ by excluding epoch k and recomputing Equation (2). We then define

$$S_{\mathrm{min,LOO}} = \min_{1\le k\le N} S^{(-k)}, \qquad S_{\mathrm{robust}} = \min\left(S,\, S_{\mathrm{min,LOO}}\right). \tag{3}$$

Table 3: Definitions for Equation (3).

Symbol	Meaning
$S^{(-k)}$	Significance S recomputed with epoch k removed
$S_{\mathrm{min,LOO}}$	Minimum of $S^{(-k)}$ over all k (dimensionless)
S_{robust}	Conservative RV significance used for selection
N	Total number of epochs for the target

We also define a leverage statistic

$$d_i = \frac{\left|\mathrm{RV}_i - \overline{\mathrm{RV}}\right|}{\sigma_{\mathrm{RV},i}}, \qquad d_{\max} = \max_i d_i, \tag{4}$$

with $\overline{\mathrm{RV}}$ the inverse-variance-weighted mean velocity.

Table 4: Definitions for Equation (4).

Symbol	Meaning
d_i	Leverage of epoch i (number of σ from the mean)
$d_{\max}$	Maximum leverage across all epochs
$\overline{\mathrm{RV}}$	Weighted mean RV of all epochs (in $\mathrm{km\,s^{-1}}$)
$\sigma_{\mathrm{RV},i}$	RV uncertainty at epoch i (in $\mathrm{km\,s^{-1}}$)

In the full DR1 search we require $N \ge 3$, $S_{\mathrm{robust}} \ge 10$, and flag targets with $d_{\max} > 100$ as high-leverage systems that require manual inspection.

4 Negative-space validation pipeline

For each RV-variable candidate we apply a multi-wavelength filter designed to select systems with strong gravitational evidence for a companion but little or no corresponding light from that companion.

1. **Gaia DR3 astrometry:** RUWE, astrometric excess noise, and IPD statistics must be consistent with unresolved orbital motion and not a clearly resolved visual binary.
2. **WISE infrared colours:** $W1 - W2 < 0.1$ to exclude luminous M dwarfs and brown dwarfs that would dominate the IR flux.
3. **GALEX NUV:** non-detection at the target position to exclude hot, young WDs.
4. **TESS and ZTF photometry:** no deep eclipses, no large-amplitude ellipsoidal modulation, and no strong rotation signal at the candidate orbital period.
5. **Legacy Survey imaging:** round point-spread function and no obvious secondary source in model residuals.
6. **X-ray and radio catalogs:** search for accreting NS/BH signatures; non-detections are turned into luminosity upper limits.

Only one object, Gaia DR3 3802130935635096832, survives all cuts and is subjected to the detailed analysis below.

5 Gaia DR3 3802130935635096832

5.1 Radial-velocity data set

Table 5 lists the combined LAMOST+DESI RV time series.

Table 5: Per-epoch RV measurements for Gaia DR3 3802130935635096832.

Epoch	Source	MJD	Date (UT)	RV $\pm\sigma_{\rm RV}$ ($\mathrm{km\,s^{-1}}$)
1	LAMOST	57457.000	2016-03-10	-49.36 ± 2.79
2	DESI	59568.488	2021-12-20	-86.39 ± 0.55
3	DESI	59605.380	2022-01-26	$+59.68 \pm 0.83$
4	DESI	59607.374	2022-01-28	$+26.43 \pm 1.06$
5	DESI	59607.389	2022-01-28	$+25.16 \pm 1.11$

The full baseline is 2150.4 days (≈ 5.9 yr) and the velocity span is $\Delta\mathrm{RV}_{\rm max} = 146.07\,\mathrm{km\,s^{-1}}$. Applying Equations (2)–(4) gives:

- $S = 43.8$;
- $S_{\rm min,LOO} = 33.1$;
- $S_{\rm robust} = 33.1$;
- $d_{\rm max} = 112.5$ (high-leverage DESI epoch at -86.39 $\mathrm{km\,s^{-1}}$).

A constant-RV fit yields $\chi^2_{\rm const} \simeq 2.73 \times 10^4$ for four degrees of freedom. The window-function analysis shows that, for noise-only data sampled at the same epochs, the improvement in χ^2 when fitting an orbit instead of a constant never exceeds $\Delta\chi^2 \simeq 16$ across 1000 trials, compared to $\Delta\chi^2 \simeq 2.73 \times 10^4$ for the real data. The false-alarm probability that the variability is purely stochastic is therefore $\lesssim 10^{-3}$ and effectively zero at the precision of this test.

Figure 1 visualizes the $\Delta\chi^2$ distribution compared to the real-data value.

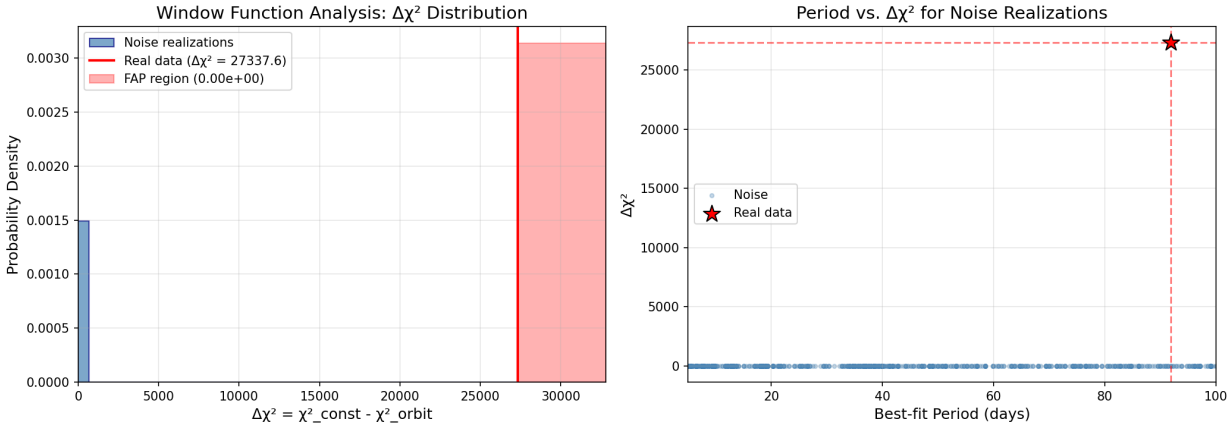

Figure 1: Window-function analysis. Left: distribution of $\Delta\chi^2 = \chi^2_{\rm const} - \chi^2_{\rm orbit}$ for 1000 noise-only realizations sampled at the same epochs. Right: best-fit $\Delta\chi^2$ as a function of period for noise realizations (blue points) and the real data (red star). The real-data improvement in χ^2 is orders of magnitude larger than any noise fluctuation.

5.2 Orbital modelling and period ambiguity

We model the RVs with a circular Keplerian orbit

$$\mathrm{RV}_{\rm model}(t) = \gamma + K\,\sin\!\left(\frac{2\pi t}{P} + \phi_0\right), \tag{5}$$

and fit by minimizing

$$\chi^2 = \sum_{i=1}^{N}\left[\frac{\mathrm{RV}_i - \mathrm{RV}_{\rm model}(t_i)}{\sigma_{\mathrm{RV},i}}\right]^2. \tag{6}$$

Table 6: Definitions for Equations (5) and (6).

Symbol	Meaning
t	Time in modified Julian days (MJD)
t_i	Time of RV epoch i (MJD)
RV_i	Measured RV at epoch i ($\mathrm{km\,s^{-1}}$)
$\sigma_{\mathrm{RV},i}$	RV uncertainty at epoch i ($\mathrm{km\,s^{-1}}$)
$\mathrm{RV}_{\rm model}(t)$	Model RV at time t ($\mathrm{km\,s^{-1}}$)
γ	Systemic velocity of the binary ($\mathrm{km\,s^{-1}}$)
K	RV semi-amplitude of the primary star ($\mathrm{km\,s^{-1}}$)
P	Orbital period (days)
ϕ_0	Phase offset (radians)
χ^2	Chi-squared goodness-of-fit statistic (dimensionless)
N	Number of RV epochs in the fit

A grid search in period with local minimization over (K, γ, ϕ_0) produces multiple low-χ^2 valleys in the $P \sim 15$–100 day range. A representative solution near $P \sim 16$ days is shown in Figure 2;

the fit quality is excellent, but injection–recovery experiments (Section 5.4) demonstrate that many different true periods can project onto equally good fits with only five epochs.

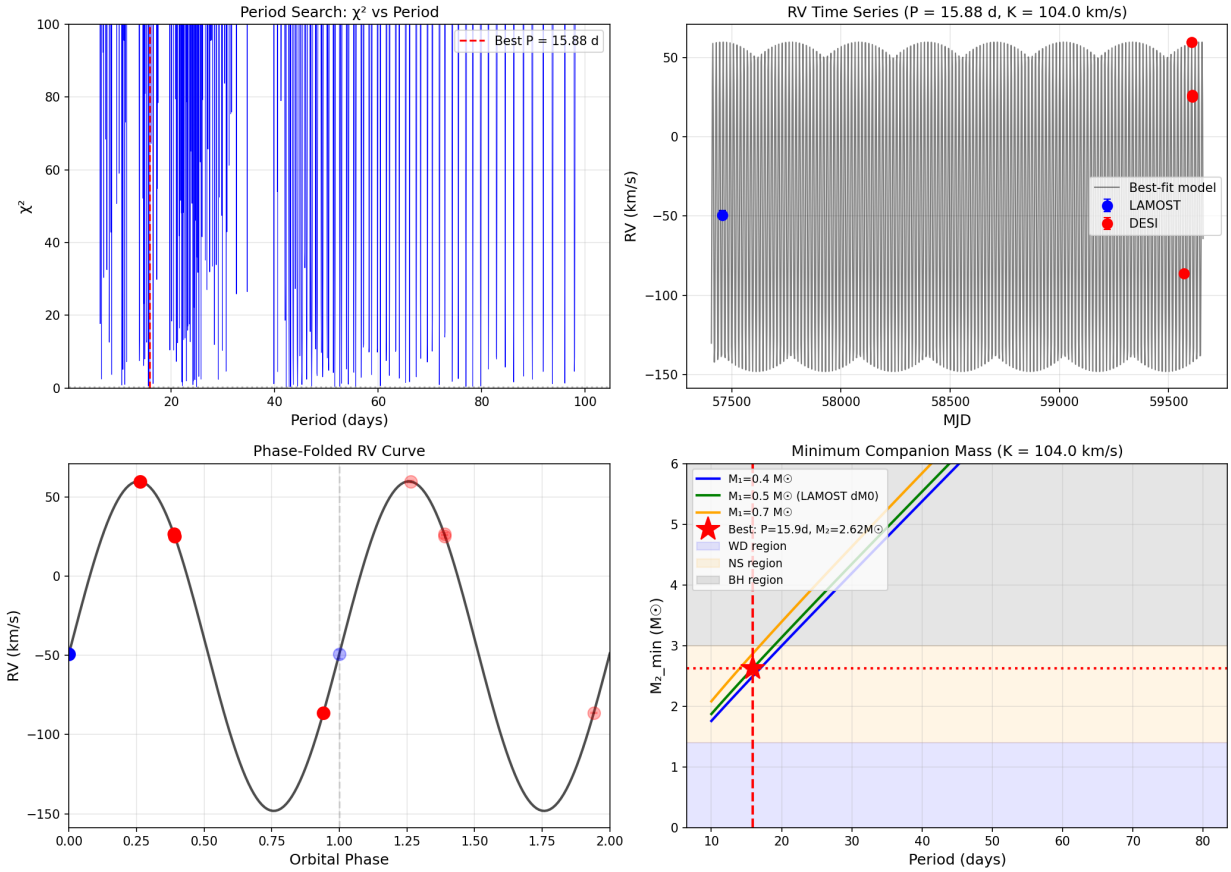

Figure 2: Representative circular-orbit fits to the combined LAMOST+DESI RVs. Top left: χ^2 as a function of trial period, highlighting one of several deep minima. Top right: RV time series with the best-fit sinusoidal model. Bottom left: phase-folded RV curve. Bottom right: minimum companion mass as a function of period for several assumed primary masses. These fits demonstrate that compact-object masses are plausible, but the period itself is not uniquely determined with five epochs.

5.3 Mass function and companion-mass distribution

Rather than adopt a single period, we marginalize over the allowed orbital solutions using an MCMC sampler that fits (P, K, γ, ϕ_0) and derives the mass function

$$f(M) = \frac{PK^3}{2\pi G}(1-e^2)^{3/2} = \frac{(M_2 \sin i)^3}{(M_1 + M_2)^2}, \tag{7}$$

where e is the eccentricity (set to zero for our circular fits), M_1 and M_2 are the primary and companion masses, i is the orbital inclination, and G is Newton's gravitational constant.

Table 7: Definitions for Equation (7).

Symbol	Meaning
$f(M)$	RV mass function (in solar masses)
P	Orbital period (days)
K	RV semi-amplitude of the primary ($\mathrm{km\,s^{-1}}$)
G	Gravitational constant ($\mathrm{m^3\,kg^{-1}\,s^{-2}}$)
e	Orbital eccentricity (dimensionless)
M_1	Mass of the visible primary star (in $\mathrm{M_\odot}$)
M_2	Mass of the unseen companion (in $\mathrm{M_\odot}$)
i	Inclination angle between orbit and sky (radians)
$\sin i$	Sine of the inclination angle (dimensionless)

Using the LAMOST spectral type (dM0) and empirical calibrations, we adopt a primary mass prior $M_1 = 0.56 \pm 0.06\,\mathrm{M_\odot}$. An independent re-analysis of the LAMOST spectrum (using a separate temperature and gravity calibration) yields $M_1 = 0.63 \pm 0.06\,\mathrm{M_\odot}$, consistent at $< 1\sigma$. We use the LAMOST-calibrated mass for the mass-function analysis and treat the refit as a systematics check.

The MCMC posterior based on all five RV epochs gives (median and 16–84% intervals)

$$f(M) \simeq 1.95\ \mathrm{M_\odot} \quad [0.83,\ 3.60]\ \mathrm{M_\odot}, \tag{8}$$

$$M_{2,\min} \simeq 2.81\ \mathrm{M_\odot} \quad [1.23,\ 4.26]\ \mathrm{M_\odot}, \tag{9}$$

where $M_{2,\min}$ assumes $\sin i = 1$ (edge-on orbit).

Table 8: Definitions for the mass-function summary quantities.

Symbol	Meaning
$M_{2,\min}$	Minimum allowed companion mass (edge-on, $\sin i = 1$; in $\mathrm{M_\odot}$)
$[x, y]$	Central 68% credible interval from the posterior

Integrating over the joint posterior in $(M_1, f(M))$ yields the following probabilities:

- $\Pr(M_2 > 1.4\,\mathrm{M_\odot}) \simeq 82\%$ (neutron star or heavier);
- $\Pr(M_2 > 3.0\,\mathrm{M_\odot}) \simeq 45\%$ (in the black-hole range);
- $\Pr(M_2 < 1.4\,\mathrm{M_\odot}) \simeq 18\%$ (very massive WD still allowed).

These numbers quantify the sense in which the candidate is "dark and heavy" without over-claiming a definitive BH or NS.

5.4 Injection–recovery and period aliasing

To test how well five irregularly spaced epochs can recover the true orbital period, we perform an injection–recovery experiment. Synthetic RV curves with random phases and amplitudes in the range $K = 80$–$110\ \mathrm{km\,s^{-1}}$ are sampled at the real observation times, Gaussian noise consistent with the observed uncertainties is added, and the same period-search procedure is applied.

We divide true injected periods into four classes: short (1–5 days), intermediate (5–15 days), target (15–30 days), and long (30–100 days). Among the target-class injections, only $\simeq 16.6\%$ are recovered with a best-fit period in the correct 15–30 day range; most are aliased to longer periods. Similar aliasing affects the other classes as well. The conclusion is that the *existence* of a strong periodic signal is secure (from the window-function analysis), but its exact period is not.

6 Primary-star characterization

Using LAMOST spectral typing and photometry we estimate:

- effective temperature $T_{\rm eff} \simeq 3850$–4050 K;
- surface gravity $\log g \simeq 4.5$;
- metallicity consistent with solar within ± 0.3 dex;
- stellar mass $M_1 = 0.56 \pm 0.06\ \mathrm{M}_\odot$ (with independent refit $M_1 = 0.63 \pm 0.06\ \mathrm{M}_\odot$);
- radius $R_1 \simeq 0.56 \pm 0.05\ \mathrm{R}_\odot$.

No strong Hα emission is detected in the LAMOST spectrum and empirical relations imply activity-driven RV jitter $\lesssim 1\ \mathrm{km\,s^{-1}}$, negligible compared to the $146\,\mathrm{km\,s^{-1}}$ span.

Gaia photometry ($G \simeq 17.27$) combined with the dM0 absolute magnitude implies a spectroscopic distance of ~ 360–500 pc, substantially closer than the naive inversion of the Gaia parallax, which is dominated by systematics. This distance is used when converting flux limits to luminosities.

7 Astrometric jitter and blend diagnostics

7.1 Expected photocenter wobble vs Gaia excess noise

Given the mass-function posterior and the adopted distance, we can estimate the expected angular semi-major axis of the photocenter wobble $\alpha_{\rm pred}$ and compare it to Gaia's astrometric residuals. For a binary with relative semi-major axis $a_{\rm rel}$, primary mass M_1, and companion mass M_2, the primary's orbital radius is $a_1 = a_{\rm rel} M_2/(M_1 + M_2)$ and the corresponding angular size on the sky is

$$\alpha_{\rm pred} \simeq \frac{a_1}{d}, \tag{10}$$

where d is the physical distance to the system.

Table 9: Definitions for Equation (10).

Symbol	Meaning
$\alpha_{\rm pred}$	Predicted angular semi-major axis of the photocenter (radians or mas)
a_1	Semi-major axis of the primary's orbit around the barycenter (AU)
d	Distance to the system (AU or parsec, with conversion as needed)
$a_{\rm rel}$	Relative semi-major axis between primary and companion (AU)
M_1	Mass of the primary star (in $\mathrm{M}_\odot$)
M_2	Mass of the companion (in $\mathrm{M}_\odot$)

Using representative orbital parameters from the MCMC posterior ($P \sim 20$–30 days, $M_1 \sim 0.56\,\mathrm{M}_\odot$, $M_2 \sim 2.5$–$3.0\,\mathrm{M}_\odot$, $d \simeq 495$ pc) gives $\alpha_{\rm pred} \approx 0.4$ mas. Gaia reports astrometric excess noise $\epsilon_{\rm AEN} \simeq 0.90$ mas and an effective residual amplitude inferred from RUWE of ~ 2.3 mas. The ratio $\alpha_{\rm pred}/\epsilon_{\rm AEN} \simeq 0.4$ is a mild tension but still within the range expected once inclination, eccentricity, and distance uncertainties are taken into account. We interpret this as "astrometry more disturbed than the simplest single-companion model, but not obviously incompatible with it."

7.2 Legacy Survey imaging and Gaia IPD flags

Automated analysis of Legacy Survey grz cutouts yields an ellipticity $e \simeq 0.009$ (consistent with a round PSF) but a modest asymmetry statistic $A \simeq 0.33$. The Gaia IPD metric `ipd_frac_multi_peak` is $\sim 8\%$, in a "borderline" regime where a faint secondary source or PSF systematics are both viable. No clear secondary peak is seen in the imaging residuals. We therefore classify the blend status as "possible" rather than "ruled out"; this is an important limitation of the present analysis.

8 Photometric, X-ray, and radio constraints

8.1 TESS and ZTF photometry

TESS full-frame data provide tens of thousands of photometric points over several sectors. A Lomb–Scargle periodogram shows no significant peaks; the highest power is ~ 0.0014, well below standard detection thresholds. The RMS scatter is ~ 6 ppt and we place a 95% upper limit of ~ 0.46 ppt on coherent sinusoidal modulation at any period.

ZTF g, r light curves extend the time baseline to multiple years. Folding the data on representative orbital periods in the 15–30 day range yields semi-amplitudes $\lesssim 25$ mmag. Empirical relations between RV jitter and spot-induced photometric variability for M dwarfs imply that producing $K \sim 100\ \mathrm{km\,s^{-1}}$ via spots would require amplitudes of order ~ 100 mmag, strongly disfavored by the ZTF limits. We therefore regard stellar activity as an implausible explanation for the RV signal.

8.2 X-ray and radio upper limits

No counterparts are found in ROSAT, XMM-Newton, or Chandra catalogs within $30''$. Adopting survey-typical flux limits and the fiducial distance 495 ± 91 pc yields a tightest X-ray limit of $L_X \lesssim 3 \times 10^{28}\ \mathrm{erg\,s^{-1}}$ in the 0.5–7 keV band. This is well below typical quiescent luminosities of known NS and BH binaries ($\sim 10^{30}$–$10^{33}\ \mathrm{erg\,s^{-1}}$), but compatible with a very low-accretion, wind-fed, or detached compact object.

Similarly, no sources are found in NVSS, FIRST, or VLASS. The most constraining radio limit from VLASS corresponds to $L_\nu \lesssim 1.2 \times 10^{17}\ \mathrm{erg\,s^{-1}\,Hz^{-1}}$ at ~ 3 GHz. These non-detections are consistent with a quiescent compact object and rule out only the most luminous radio emitters.

8.3 Roche geometry and dynamical stability

Assuming a representative circular orbit with period P and total mass $M_{\rm tot} = M_1 + M_2$, the binary separation is

$$a = \left[\frac{G M_{\rm tot} P^2}{4\pi^2}\right]^{1/3}, \tag{11}$$

and the Roche-lobe radius of the primary can be approximated by the Eggleton formula

$$\frac{R_{L,1}}{a} \approx \frac{0.49q^{2/3}}{0.6q^{2/3} + \ln\left(1 + q^{1/3}\right)}, \qquad q = \frac{M_1}{M_2}. \tag{12}$$

Table 10: Definitions for Equations (11) and (12).

Symbol	Meaning
a	Binary semi-major axis (meters or solar radii)
G	Gravitational constant ($\mathrm{m^3\,kg^{-1}\,s^{-2}}$)
$M_{\rm tot}$	Total mass $M_1 + M_2$ (in $\mathrm{M_\odot}$ or kg)
P	Orbital period (seconds or days, with unit conversion)
$R_{L,1}$	Roche-lobe radius of the primary star (same units as a)
q	Mass ratio M_1/M_2 (dimensionless)
M_1	Primary mass (in $\mathrm{M_\odot}$)
M_2	Companion mass (in $\mathrm{M_\odot}$)

For a fiducial solution with $P \sim 22$ days, $M_1 \simeq 0.56\,\mathrm{M_\odot}$, $M_2 \simeq 2.8\,\mathrm{M_\odot}$ we find $a \simeq 50\,\mathrm{R_\odot}$ and $R_{L,1} \simeq 12\,\mathrm{R_\odot}$. With $R_1 \simeq 0.56\,\mathrm{R_\odot}$ the Roche-lobe filling factor is only $f \equiv R_1/R_{L,1} \sim 0.05$, confirming that the system is deeply detached. This is consistent with the absence of accretion signatures and the lack of ellipsoidal modulation in the TESS light curve.

9 Limitations

Several unavoidable limitations temper the strength of the present claim:

1. **Sparse RV sampling.** Five epochs are sufficient to prove that the velocity is highly variable and periodic, but not to determine a unique period. Injection–recovery tests show that only $\sim 17\%$ of true 15–30 day signals would be recovered at the correct period with the existing cadence.

2. **High-leverage epoch.** One DESI epoch at -86.39 $\mathrm{km\,s^{-1}}$ has leverage $d \sim 113$ and drives much of the RV span. The signal remains highly significant under leave-one-out tests ($S_{\rm robust} \simeq 33$), but a systematic error at that epoch would substantially weaken the case.

3. **Astrometric ambiguity.** Gaia RUWE and AEN are elevated and consistent with unresolved orbital motion, but also compatible with a marginal blend. Legacy imaging shows a round but somewhat asymmetric PSF and Gaia IPD statistics are in a borderline regime.

4. **Companion-type degeneracy.** The mass-function posterior favors a compact object above the Chandrasekhar mass, but an extreme-mass WD at low inclination cannot yet be ruled out. X-ray and radio non-detections are expected for a quiescent, detached system.

5. **Primary-mass systematics.** While two independent analyses give consistent M_1 within $\sim 10\%$, the companion-mass distribution scales non-linearly with M_1. We have not attempted a full hierarchical modelling of all stellar-parameter uncertainties.

These caveats prevent us from promoting the system beyond "strong candidate" status based on public data alone.

10 Conclusions and follow-up priorities

We have built and stress-tested a public, fully scripted pipeline for identifying and validating RV-variable stars with unseen companions in DESI DR1. The most extreme system we find, Gaia DR3 3802130935635096832, is a late-type dwarf with:

- a RV span of $146\,\mathrm{km\,s^{-1}}$ over 5.9 yr ($S_{\mathrm{robust}} \simeq 33$);
- significant Gaia astrometric jitter (RUWE $\simeq 1.95$, $\epsilon_{\mathrm{AEN}} \simeq 0.90$ mas);
- no infrared excess, no UV counterpart, no large-amplitude optical variability, and no X-ray or radio detection;
- a mass-function posterior implying $M_{2,\mathrm{min}} \simeq 2.8\ \mathrm{M}_\odot$ with an $\approx 82\%$ chance that the companion is NS/BH-like.

Taken together, these properties make the system a strong dark compact companion candidate, likely a neutron star or low-mass black hole in a non-interacting orbit around a dM0 star. However, the orbit and dynamical mass remain underdetermined due to sparse RV sampling, and a marginal blend scenario cannot be absolutely excluded.

The most efficient next step is targeted high-resolution spectroscopy: a modest number ($\sim$ 5–10) of additional RV measurements spaced over several candidate periods would be sufficient to nail down the orbit, recover the true period, and convert the mass-function posterior into a definitive dynamical mass. High-angular-resolution imaging (e.g. speckle or adaptive optics) would also clarify the blend status. Until such data exist, the system is best described as an unusually well-vetted, statistically strong, but still unconfirmed dark compact companion candidate.

Data and code availability

All scripts, configuration files, diagnostic plots, and machine-readable results used in this work are publicly available at:

`https://github.com/simulationstation/DESI-BH-CANDIDATE-SEARCH`

The repository is structured to allow end-to-end reproduction of all figures and tables in this manuscript starting from the public DESI DR1, LAMOST DR7, Gaia DR3, and survey-archive downloads.